Modelling impacts of spatially variable erosion drivers on suspended sediment dynamics

Giulia Battista[1], Peter Molnar[1], and Paolo Burlando[1]

[1]Institute of Environmental Engineering, ETH Zurich, 8093 Zurich, Switzerland

Correspondence: Giulia Battista (battista@ifu.baug.ethz.ch)

Abstract.

The estimate of suspended sediment load in rivers is difficult, because sediment production and transport process at the catchment scale are strongly variable in space and time. Among the sources of this variability are the spatially distributed nature of overland flow as an erosion driver, and of surface erodibility given by soil type and vegetation cover distribution. Temporal variability mainly results from the time sequence of rainfall intensity during storms and snowmelt leading to soil saturation and overland flow.

We present a new spatially distributed soil erosion and suspended sediment transport module integrated in the computationally efficient physically based hydrological model TOPKAPI-ETH, with which we investigate the effects of the two erosion drivers - precipitation and surface erodibility - on catchment sediment fluxes in a typical pre-alpine mesoscale catchment. By conducting a series of numerical experiments, we quantify the impact of spatial variability of the two key erosion drivers on erosion-deposition patters, sediment delivery ratio, and catchment sediment yields.

Main findings are that the spatial variability of erosion drivers affects sediment yield by (i) increasing sediment production due to a spatially variable precipitation, while decreasing it due to a spatially variable surface erodibility, (ii) favoring the clustering of sediment source areas in space, and (iii) decreasing their connectivity to the river network by magnifying sediment buffers. The results highlight the importance of resolving spatial gradients controlling hydrology and sediment processes when modelling sediment dynamics at the mesoscale, in order to capture the key effects of sediment sources, buffers, and hillslope hydrological pathways in determining the sediment signal.

1 Introduction

Fine sediment produced in catchments by upland erosion and transported by rivers as suspended load is an important part of the global sediment budget (e.g. Peucker-Ehrenbrink, 2009) and an important driver of water quality and aquatic biota in rivers (e.g. Bilotta and Brazier, 2008). Human activity strongly interacts with the natural processes of suspended sediment production and transport, on the one hand by practices that enhance soil erosion, like agriculture, mining and deforestation, and on the other hand with the construction of sediment retention structures such as dams (e.g., Syvitski et al., 2005; Montgomery, 2007; Syvitski and Kettner, 2011; Borrelli et al., 2017). In the context of enhanced soil erosion, phenomena like the loss of soil productivity, the reduction of water quality due to higher turbidity and concentration of pollutants, and accelerated reservoir

siltation are expected (e.g. Pimentel et al., 1987; Davies-Colley and Smith, 2001). The combined effect of enhanced soil erosion and sediment retention by dams modifies the river sediment equilibrium and can result in river incision in the case of sediment starvation, contributing to undermine the stability of bridges and other infrastructures, and leading to coastal erosion (Kondolf, 1997; Chen and Zong, 1998; Schmidt and Wilcock, 2008). The opposite case of excessive sediment load in rivers may also lead to an increase in flood risk in alluvial floodplains due to sediment deposition (Yu, 2002; Walling, 2006; Rickenmann et al., 2016). The intensity of these effects is expected to grow in the future, as the magnitude and number of highly erosive extreme precipitation events are foreseen to increase in some parts of the world due to climate change and anthropic influence on land cover increases (e.g. Yang et al., 2003; Nearing et al., 2004; Peleg et al., 2019). Therefore, the monitoring and understanding of suspended sediment dynamics is essential to explain how disturbances produced by such human interventions may affect the sediment balance.

Fine sediment yield in rivers is usually estimated from intermittent measurements of sediment concentration by means of sediment-discharge rating curves (see Gao (2008) for a review). However, the development and use of these curves is often highly problematic because of the strong non-uniqueness of suspended sediment concentrations (SSCs), especially in small to medium sized catchment (up to 1000 km^2). Here, the same value of discharge (Q) often leads to a wide range of SSCs, producing highly scattered SSC-Q rating curves (e.g., Walling, 1977; Walling and Webb, 1982; Ferguson, 1986; Asselman, 2000; Horowitz, 2003). The strong variability in SSC is attributed to the high non-linearity of the sediment production and transport processes in time and space, and the presence of threshold and feedback mechanisms in sediment mobilization and transfer (e.g., Asselman, 1999; Collins and Walling, 2004; Seeger et al., 2004; Fryirs et al., 2007; Bracken et al., 2015).

Temporal and spatial variability in suspended sediment transport can originate from several sources (see Vercruysse et al. (2017) for a review). Among the sources of temporal variability, the role of hydrometeorological conditions (rainfall, antecedent wetness conditions and runoff) has been widely investigated, with a particular focus on the shape and direction of the hysteresis loops of the SSC-Q relation (Smith et al., 2003; Seeger et al., 2004; Zabaleta et al., 2007; Duvert et al., 2010; Dominic et al., 2015; Misset et al., 2019). Other sources of variability are the exhaustion of preferential sediment sources, the activation of new ones, and changes in the connectivity of such sources to the river network. These aspects have been studied for example as consequences of land use change and flow regulation (Olarieta et al., 1999; Siakeu et al., 2004; Costa et al., 2018). Variability of sediment transport in space depends on the distribution of sediment sources within the catchment, the catchment sediment connectivity, and the efficiency of sediment transport within the stream network. Wass and Leeks (1999) related differences in sediment loads across the basin to geomorphic and climatic gradients, while Fryirs and Brierley (1999) and Lang et al. (2003) reconstructed the change of sediment sources in time and their coupling with the channels. The problem of catchment sediment connectivity has been addressed from a conceptual point of view, by introducing the ideas of structural and functional connectivity, to distinguish between the physical connection among landscape units and the connectivity generated by the system process interactions (Wainwright et al., 2011; Fryirs, 2013; Bracken et al., 2015). Based on these concepts, several indices have been introduced to assess sediment connectivity in a river basin (see Heckmann et al. (2018) for a review).

The above studies highlight the need to account for both types of variability (temporal and spatial) in order to investigate basin sediment dynamics. Including this variability is especially important at the medium and large catchment scale and in

mountainous environments, where the gradients of climatic and physiographic variables are most relevant. Few studies have focused specifically on the impacts of spatially variable erosion drivers on suspended sediment dynamics in such environments. A systematic investigation of this research gap can be performed by means of numerical models that include the main hydrological processes, their temporal dynamics and distribution in space, as well as their interaction with the topography and morphology of the basin. Several existing models are partially suitable for this task. The main limitations are that many are only suitable for event-applications (Answers (Beasley et al., 1980), KINEROS (Woolhiser et al., 1990), WEPP (Nearing et al., 1989)) or present simplified hillslope hydrology and runoff formation solutions, as in the case of WATEM/SEDEM (Van Rompaey et al., 2001), landscape evolution models, e.g. Caesar-Lisflood (Coulthard et al., 2013), SIBERIA (Hancock et al., 2000), or some large-scale sediment flux models, e.g. WBMsed (Cohen et al., 2013) and Pelletier (2012). More suitable approaches are tRIBS (Francipane et al., 2012), which includes physically based hydrological component suitable for long-term process simulations, and DSHVM (Doten et al., 2006), which features a detailed hydrology-vegetation component and sediment module. However, the number of processes represented in these two models, requires a high computational power and their applications have so far been limited to small basins and/or short time scales. Finally, Tsuruta et al. (2018) present a spatially distributed model especially for large basins, which, being based on a land-surface model, features an approximated coarse-scale representation of hydrological and sediment connectivity on the hillslopes.

In this work, we present a new modelling approach especially suitable for alpine catchments with highly variable climate and complex topography, that integrates a new spatially distributed soil erosion and suspended sediment transport module within the computationally efficient, physically based hydrological model TOPKAPI-ETH (Fatichi et al., 2015). The model combines unsteady simulation of surface and subsurface water fluxes with a simple hillslope erosion and sediment transport component. The sediment component is simple by design, to avoid over-parameterization and to maintain computational efficiency enabling applications to medium and large catchments. The model allows continuous high spatial resolution (Δx=100 m) simulations to track overland flow and hillslope sediment transport by local changes in soil moisture dynamics produced by rainfall, snowmelt and lateral drainage over long periods of time. The model also allows high temporal resolution (Δt=1 hr) simulations that capture fast runoff response to the hydrological drivers, which, together with the topographically driven flow routing, reproduces the connectivity of water and sediment pathways in the catchment over time.

The overall aim of this research is to provide a state-of-the-art catchment hydrology-sediment modelling framework to better understand the sources of variability in suspended sediment concentrations and their effects on predictions of sediment yield. Accordingly, we conducted numerical experiments on a mesoscale pre-alpine river basin, where we turned on and off the spatial variability in two key erosion drivers - rainfall and surface erodibility - to quantify their individual and combined effect on suspended sediment mobilization and transfer. We address the following specific research questions: (RQ1) Does fully distributed physically-based hydrology-sediment modelling predict variability in SSC-Q relations that is in agreement with observations? We argue which key hydrological processes are needed in such a model and why. (RQ2) Can we identify the location of sediment sources and quantify their productivity and connectivity with such a modelling approach? We assess the effect of the spatial distribution of rainfall and surface erodibility on hillslope erosion-deposition patterns and sediment mobilization and we quantify the sediment source connectivity to the river network by analysing the sediment delivery ratio

along the main stream and in tributaries. (RQ3) Is the effect of spatially distributed erosion drivers visible in sediment yield at the catchment outlet? We show how integration of the spatially variable inputs in space impacts sediment yield under different scenarios.

2 Methods

2.1 Hydrology-sediment model description

The model we present in this work is an extension of the hydrological model TOPKAPI-ETH (Fatichi et al., 2015), which we integrated with a new hillslope erosion and channel suspended sediment flow module. The TOPKAPI-ETH hydrological model was chosen because of its spatially distributed nature and physically based representation of the major hydrological processes, combined with a reasonably contained computational demand. The model is based on a regular square grid discretization in space and a 3-layer vertical discretization of the subsurface. The river network is identified in the domain by means of a flow accumulation algorithm based on the topography. The transition between hillslope and channel process description, i.e. the beginning of the model river network, is set by a user-defined critical upstream area, or river initiation threshold RT, above which water flow is modelled as channel flow. Each river network cell can be fully or partially covered by the stream, depending on the actual stream width and grid cell resolution.

In TOPKAPI-ETH surface and subsurface flow is simulated by the kinematic wave approximation, with resistance to flow given by surface roughness and soil transmissivity as a function of soil properties. Water may saturate the soil locally and lead to overland flow generation by saturation excess or by infiltration excess in case of high rainfall intensities. Soil is dried by evapotransporation, lateral drainage and percolation to groundwater storage. The model includes snow cover accumulation and melt, which are important in the water balance of alpine basins. For further details about the model see Fatichi et al. (2015). TOPKAPI-ETH allows long-term, high resolution simulations (time step Δt=1hr, grid size Δx=100 m) in medium and large catchments (>1000 km^2), even when integrated with a sediment mobilization and transfer component, since the kinematic wave approximation of the surface and subsurface flow routing are solved analytically, thus keeping the model computationally efficient (Liu and Todini, 2002).

In the new sediment module of TOPKAPI-ETH, the mobilization and routing of fine sediment on the hillslopes takes place by action of overland flow, which is assumed to transport sediment at its maximum capacity. As a consequence, deposition and erosion can occur on the hillslopes at a rate D [kg m^{-3} s^{-1}] depending on the hydraulic and topographic properties of the cells along the flow path:

$$D = \nabla \cdot q_s, \tag{1}$$

where q_s [kg m^{-2} s^{-1}] is the overland flow transport capacity, modelled following Prosser and Rustomji (2000) as a function of the specific overland flow discharge q [m^3 s^{-1}] and the surface slope S:

$$q_s = \alpha q^\beta S^\gamma, \tag{2}$$

where β and γ are transport exponents, and α [kg s$^{0.4}$ m$^{-4.8}$] is a calibration parameter that captures the effect of land surface and soil properties on erosion and sediment transport. The sediment flux q_s is directed to the downstream cell with the steepest gradient. Sediment inflow into a cell can be from one or more upstream cells.

130   Once the sediment mobilized and routed on the hillslopes reaches the channel, it is assumed to move as suspended sediment load. The suspended sediment flux in the river network is treated as an advection process and solved with the same numerical methods used for water flow. The 1D equation of suspended sediment flux in the channel, integrated over the river cross-section, is:

$$\frac{\partial AC}{\partial t} = E - \frac{\partial QC}{\partial x}, \tag{3}$$

135   where Q [m^3 s^{-1}] is the river discharge, C [g m^{-3}] is the SSC, A [m^2] is the cross-section area of flow and E [g m^{-1} s^{-1}] represents the exchange of sediment with the bed and local sediment sources. By following the reasoning of Liu and Todini (2002), Equation 3 can be integrated along the length of the grid cell (i.e. in the flow direction), within which the values of the variables are assumed to be constant, and then solved analytically as a first-order ordinary differential equation:

$$\frac{\partial V_i C_i}{\partial t} = E_i X + Q_{in} C_{in} - \frac{U_i}{X} C_i V_i, \tag{4}$$

140   where X [m] is the length of the grid cell size, V_i [m^3] the volume of water inside a cell ($V_i = A_i X_i$), U_i [m s^{-1}] the mean flow velocity, C_i and E_i are the mean values of C and E inside the grid-cell. Q_{in} and C_{in} are the discharge and sediment concentration entering the cell i from the upstream grid cell $(i-1)$.

2.2   Study site

To investigate the research questions outlined above, we chose the Kleine Emme river basin, a pre-alpine catchment located in
145   central Switzerland, because here the natural regime of water and sediment flow is almost unaltered. The basin has an area of 477 km^2, an elevation range of 430-2300 m. a.s.l. and a mean annual precipitation of 1650 mm (Figure 1a). The mean annual discharge at the outlet is 12.6 m^3/s. The catchment is mostly natural, with more than 50% of the catchment surface covered by forest and grassland (Figure 1c). No use of water for irrigation or hydropower is known and sediment-retaining infrastructures are absent. Moreover, the absence of glaciers means that fine sediment production in the basin is mostly driven by overland
150   flow and rainfall processes. Finally, the diverse geomorphology of the basin has been subject of several studies and long-term estimates of denudation rates are available (e.g., Schlunegger and Schneider, 2005; Schwab et al., 2008; Dürst Stucki et al., 2012; Van Den Berg et al., 2012; Clapuyt et al., 2019).

Measurements of precipitation, air temperature and sunshine duration are available from automatic weather stations located inside or in the vicinity of the basin operated by MeteoSwiss. The information about the spatial distribution of precipitation
155   inside the basin area is available from the 1x1 km daily gridded product of MeteoSwiss RhiresD (Frei and Schär, 1998; Schwarb, 2000). Streamflow is monitored at Werthenstein and at the basin outlet by the Federal Office of the Environment (FOEN) and at Sörenberg by the Canton Luzern (Figure 1a). FOEN also provided the cross section measurements for the main channel of the river and measurements of suspended sediment concentration. SSCs have been manually sampled at the outlet
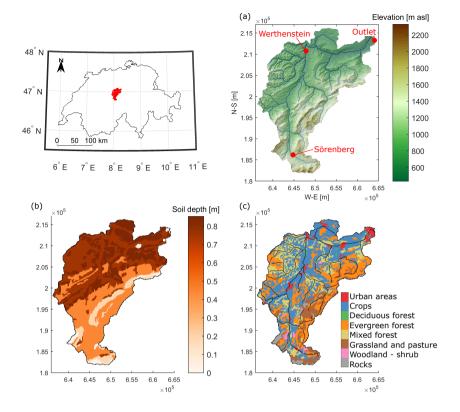
Figure 1. (a) Digital Elevation Model (DEM) of the Kleine Emme basin and location of discharge gauges (source SwissAlti3D, 2017), (b) Soil depth, derived from the Swiss soil map (Bodeneignungskarte, 2012), (c) Land cover derived from Corine Land Cover map (CLC, 2014).

since 1974, but with a regular frequency of two samples a week only since 2004. Because of the low temporal resolution of these measurements, which is typical of many river sediment monitoring networks, we expect this dataset to miss extreme SSCs generated by flood events or very localized sediment sources. Finally, the information about soil type and depth for the basin is available from the soil map of Switzerland (Bodeneignungskarte, 2012) (Figure 1b) and land cover is provided by the Corine Land Cover dataset (Figure 1c).

2.3 Model setup and calibration

2.3.1 Hydrology

Given the period of availability of suspended sediment measurements in the Kleine Emme, the simulation was set up for the years 2003 to 2016, where the first year is considered a warm-up period. The meteorological input data required by the hydrological component of TOPKAPI-ETH are hourly precipitation, air temperature and cloud cover. The precipitation input file was created by combining station and gridded precipitation datasets following the approach of Paschalis et al. (2014). In this approach hourly precipitation measured at the rain gauges was spatially interpolated to match the spatial distribution
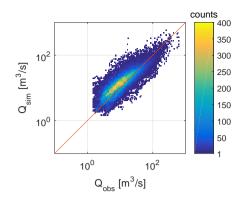
Figure 2. Performance of the hydrological model: density plot of observed vs simulated hourly discharges at the outlet of the river basin for the period 2004-2016.

of the daily precipitation reported by the gridded RhiresD dataset. The hourly time series of measured air temperature were extrapolated across the model domain to different elevations with a temperature lapse rate of -5.5 °C/km. The cloud cover transmissivity was derived from the hourly sunshine duration measurements following the empirical relation proposed by Kasten and Czeplak (1980).

175   The model was run at a Δx=100 m spatial resolution and a constant time step Δt=1 hour. To initiate the model calibration, realistic values of the hydrological parameters were assigned based on the soil characteristics and previous investigations (Paschalis et al., 2014; Pappas et al., 2015). The soil hydraulic conductivity and the residual and saturation soil water content parameters were then adjusted in order to maximize the performance of the hydrological model in terms of correlation coefficient (r), Nash-Sutcliffe efficiency (NSE) and root mean square error (RMSE) for discharge measured at three streamflow

180   gauging stations.

     The final configuration of the hydrological model performed very well in reproducing the observed discharge at the outlet and at Werthenstein (see Table 1 and Figure 2). Discharge data are available at a sub-daily resolution at Sörenberg only from the year 2005, therefore the evaluation of the performance at this station does not consider the first year of simulation. The model performance at this station is slightly worse, probably also due to the lower accuracy of the measurements, but still

185   satisfactory.

2.3.2   Setup of the sediment module

The inputs needed to run the hillslope erosion and suspended sediment transport modules are the parameters α, β and γ in Equation 2. The β and γ parameters are assumed spatially uniform and equal to 1.4, following Prosser and Rustomji (2000). The parameter α contains information about the soil and land surface properties that influence the rate of soil erosion. We

190   derived the spatial distribution of α by the product of the soil erodibility parameter K of the Universal Soil Loss equation (USLE), computed for Switzerland by Schmidt et al. (2018), and the land use USLE parameter C, which we derived from Yang et al. (2003) (see Figure S1). In this way we implicitly account for the influence of particle size distribution, organic

Table 1. Hydrological performance for the simulation period 2004-2016 at the three flow monitoring stations in terms of correlation coefficient (r), Nash-Sutcliffe efficiency (NSE) and root mean square error (RMSE) for data simulated at the hourly resolution and aggregated to daily, monthly and annual values.

	Outlet			Werthenstein			Sörenberg (2005-16)		
	r	NSE	RMSE $[m^3/s]$	r	NSE	RMSE $[m^3/s]$	r	NSE	RMSE $[m^3/s]$
Hour	0.84	0.69	0.75	0.84	0.65	0.74	0.63	0.72	1.43
Day	0.91	0.80	0.53	0.90	0.78	0.52	0.80	0.56	0.83
Month	0.93	0.76	0.28	0.92	0.77	0.26	0.88	0.77	0.38
Year	0.93	-	0.18	0.92	-	0.13	0.79	-	0.10

matter content, soil structure, permeability, surface roughness and vegetation cover in determining the spatial distribution of surface erodibility. A comparable approach is proposed by Hancock et al. (2017).

195   The ratio between the product of C and K of the different classes was then kept constant in the calibration process and α was calibrated by multiplying the CK values by a spatially constant parameter α_1:

$$\alpha(x,y) = \alpha_1 C(x,y) K(x,y), \tag{5}$$

where x and y are coordinates in space. With respect to channel processes, the water column-bed exchange and local sediment source term E in equation 3 is unknown. In the Kleine Emme significant deposits of fine sediment in the river bed

200   are not present and bedrock is often exposed, indicating an efficient fine sediment transport downstream (Schwab et al., 2008). Furthermore, the infrequent SSC measurements do not allow to quantify the term explicitly. This leads us to assume that $E=0$ for this river. However, by setting $E=0$ we neglect also local sediment sources along the channels, which is probably an approximation of the sediment production processes of the specific case study. Also on the hillslopes, localized sediment sources are not explicitly modelled and are present only insofar they are represented by high C and K values. The lack of

205   explicit inclusion of point sediment sources and their modelling is a limitation of the current approach, which we will address in future work.

2.3.3   Calibration of the sediment module

We found that the parameters that have the highest influence on matching the observed SSC at the outlet are the river initiation threshold RT, i.e. the extension of the modelled river network, and the α_1 constant, defining the soil erodibility. RT has a

210   small influence on discharge, as shown by Table S1, while it is a relevant parameter for the modelling of hillslope erosion and sediment transport. Since fine sediment mobilization can only take place on the hillslopes, the extension of the channels onto
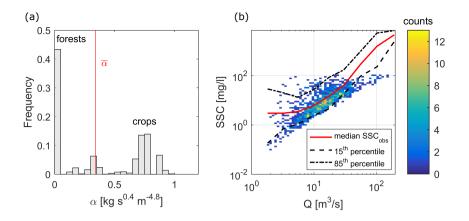
Figure 3. (a) Frequency distribution of the calibrated surface erodibility parameter α, with mean α indicated with the red line; (b) density plot of the simulated SSC at outlet compared with measurements, the lines show the median (red) and 15th and 85th percentile (black dashed) of the observations.

the hillslopes influences the magnitude of the sediment input into first-order channels and subsequently downstream through the river network.

In the calibration of the model we focused on the lowest 85th percentile of the measurements, because flood events in the SSC data are likely under-sampled, due to the monitoring strategy, and the model is expected to underestimate the SSC extremes due to the simplified representation of sediment mobilization processes. The calibration was performed by matching the trend and the dispersion of the measured and modelled SSC-Q cloud of points. This was done by visual matching and by comparing the mean and variance of the observed SSCs. The final calibrated parameters are α_1=0.0138 kg m$^{-1.8}$ s$^{-2.6}$ and RT=0.4 km^2. The histogram of α and its spatial distribution are shown in Figures 3a and 7d, respectively; the spatial mean of α is 0.3412 kg s$^{0.4}$ m$^{-4.8}$. We note that the calibrated river initiation threshold is very close to the drainage area that Schlunegger and Schneider (2005) propose as the threshold area at which channelized processes start dominating over hillslope processes in the development of the landscape in this study basin (0.1-0.2 km^2).

Using this parameterization, the measured SSC-Q cloud of points is captured very well for moderate discharges (Figure 3b), whereas the concentrations at highest discharges are underestimated, as expected. Overall, 90.4% of the simulated SSCs fall within the 5th and 95th percentile of the observations and, if the simulated SSCs are sampled at the hours of observations and compared to the observations limited to their 85th percentile, the observed SSC mean and variance are reproduced with very small errors ($\overline{SSC}_{sim} = 12.40\ mg/l$, $\overline{SSC}_{obs} = 12.20\ mg/l$; $\sigma^2_{sim} = 210.47\ mg/l$, $\sigma^2_{obs} = 233.15\ mg/l$) (Figure S2). We attribute the underestimation of high sediment concentrations (above 85th percentile) to missing localized sediment sources, i.e. mass wasting processes in the model, which are responsible for point sediment sources, like landslides, debris flows and bank erosion.

3 Erosion driver numerical experiments

In order to investigate the processes leading to the scatter in the SSC-Q relation and how they affect the spatial organization of sediment transport, we performed simulation experiments that quantify the role of spatial variability in two key erosion drivers - precipitation and surface erodibility. Precipitation is the main hydrological driver of hillslope erosion through the overland flow term q^β in Equation 2, while surface erodibility is represented by the parameter α in Equation 2.

We designed four numerical experiments by combining spatially variable and/or uniform distributions of the two erosion drivers (Figure 4). The reference experiment (SIM 1) accounts for the highest level of complexity by considering both precipitation and erodibility variable in space. This is the experiment with which the model was calibrated (see section 2.3.3). The second experiment (SIM 2) aims to quantify the role of the spatial variability in precipitation, by reducing it to be uniformly distributed in space. The temporal variability was preserved by setting the hourly precipitation in each cell equal to the mean hourly distributed precipitation over the catchment. The third experiment (SIM 3) is designed to investigate the role of the spatial variability in surface erodibility by reducing it to uniform surface erodibility throughout the basin, equal to the mean value of the calibrated spatial distribution of α. A fourth experiment (SIM 4), where the spatial variability in both drivers was reduced to uniform, was run to quantify the combined effect of the two erosion drivers.

4 Results

In this chapter, in section 3.1 we evaluate the spatio-temporal variability in sediment mobilization and transport and the scatter of the SSC-Q relation it produces by the fully distributed erosion drivers in SIM 1 (RQ 1). The spatial distribution of suspended sediment transport is then evaluated in subsequent sections and related to the hydrological response of the basin (RQ 2). Here we compare the activation of sediment sources and the sediment mobilization in the four simulations (section 4.2) and we quantify the connectivity of sediment transfer by means of the sediment delivery ratio (section 4.3). Finally, in section 4.4, we analyze the sediment load at the outlet as a function of the sediment spatial properties observed in the different scenarios (RQ3).
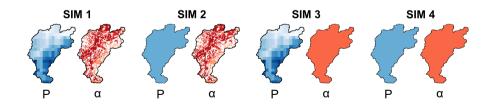
Figure 4. Summary of model runs: in SIM 1 sediment mobilization and transfer are driven by a spatially distributed precipitation (P) and surface erodibility (α), in SIM 2 and SIM 3 the spatial variability in precipitation and surface erodibility have been removed, respectively, and in SIM 4 both spatial variabilities have been removed.

4.1 Spatio-temporal variability in erosion and sediment transport

The modelled scatter in the SSC-Q relation in SIM 1 explains about 30% of the measured concentration range for discharges up to the 85th percentile, while it shows a much more significant underestimation for the highest flows (Figure 3b). For a comparison between the SSC-Q scatter generated by the different scenarios of erosion drivers, the reader is referred to Figures S4 and S5. In the following we analyse the sources of this variability, by showing the time series of discharge, the sediment load and concentration for one representative year (Figure 5a) and by analysing the pattern of erosion and deposition across the basin from the entire simulation period (Figure 5b).

High sediment fluxes in April and May, which are evident both in observations and in the model (Figure 5), indicate the contribution of snowmelt to discharge and the erosion of the surface by widespread overland flow. Summer events (storms) provide a small contribution to the yearly sediment yield, however, they generate some of the highest sediment concentrations in the model even though the runoff remains low. As expected, high SSCs are not observed in the measurements during summer, because sediment is rarely sampled during summer floods (see section 2.2). In winter months, snow covers the majority of the catchment and maintains the sediment flux very close to zero in both observations and simulations (Figure 5a).

Most of the erosion is simulated in the south-eastern part of the basin, where slopes are steeper, soil is thinner and the highest precipitation, snow accumulation and melt occur (Figure 5b). In these regions, it is easier to saturate the soil and generate runoff over larger areas that merge and generate connected areas of overland flow, thus producing wide erosional surfaces on steep mountain flanks. Deposition is simulated at the valley bottoms or at locations of slope reduction. In the north-western part of
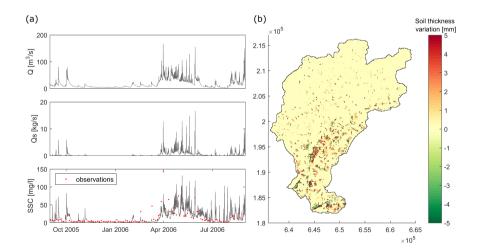
Figure 5. (a) Time series of hourly modelled discharge Q, suspended sediment load Qs and concentrations SSC for one year at the outlet. The red dots in the SSC time plot show the observed values. (b) Change in soil thickness at the end of the 13-year simulation. Positive values indicate erosion, negative values indicate deposition.
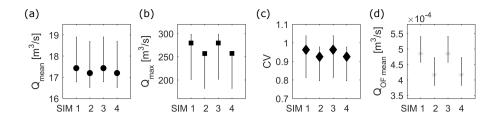
Figure 6. Comparison of the hydrological response of the basin in the four simulations: (a) mean annual discharge Q_{mean}, (b) annual flood Q_{max} and (c) the coefficient of variation CV of the hourly discharge at the basin outlet, and (d) the mean annual overland flow runoff over the basin Q_{OFmean}. The markers indicate the mean values and the lines the interval between the 25th and 75th percentile of the distribution from hourly data over the entire simulation period.

270 the basin, overland flow remains constrained to the channel headwaters due to the deeper soil and to the higher drainage density of the area. This distribution of erosion is coherent with the different geomorphological characteristics of the two areas of the basin, as further discussed in section 5.2. We observe that, because of the transport capacity approach in the hillslope transport module, areas of strong erosion are often associated with significant deposition downstream. In the following, we will refer to these areas of strong erosion as sediment source areas.

275 The mean annual suspended sediment load generated by SIM 1 is $1.42 \ 10^4$ t/y, which is significantly lower than the $2.83 \ 10^5$ t/y computed from the measurements at Littau by Hinderer et al. (2013). Consistently, the mean annual erosion rate of 0.07 mm/y underestimates the denudation rates derived from ^{10}Be samples in the Entlen and Fontanne sub-basins by Wittmann et al. (2007), Norton et al. (2008) and Van Den Berg et al. (2012) (between 0.38 and 0.52 mm/y), which are from active erosion areas and integrate over a much longer time span of about 10^4 years. The lower estimates of sediment load and erosion rates

280 by our model compared to such data is expected, given the underestimation of SSC at high flows by the model. This limitation will be further discussed in section 5.1.

4.2 Sediment sources and sediment production

To interpret the effect of the spatial variability of precipitation and surface erodibility on sediment transport, in Figure 6 we compare the hydrological response of the basin in the four simulations in terms of the mean annual discharge Q_{mean}, annual

285 flood Q_{max}, coefficient of variation CV of the hourly discharge at the basin outlet, and mean annual overland flow runoff over the basin Q_{OFmean}. Figure 6 indicates that uniform precipitation (SIM 2 and 4) is less efficient in producing runoff (Q_{mean}, Q_{max} and Q_{OFmean}) and therefore has a lower erosive power. Spatially variable precipitation (SIM 1 and 3) produces a greater flow variability, because it allows to distinguish between convective rainfall patterns, which affect confined regions of the basin with a specific hydrological response, and stratiform rainfall patterns which affect the entire basin with lower precipitation

290 intensities.

The sediment response of the basin in the four simulations is compared in the following by looking at the distribution of sediment source areas and their productivity. Figure 7 compares soil thickness variation in SIM 2 and 3 respectively to SIM
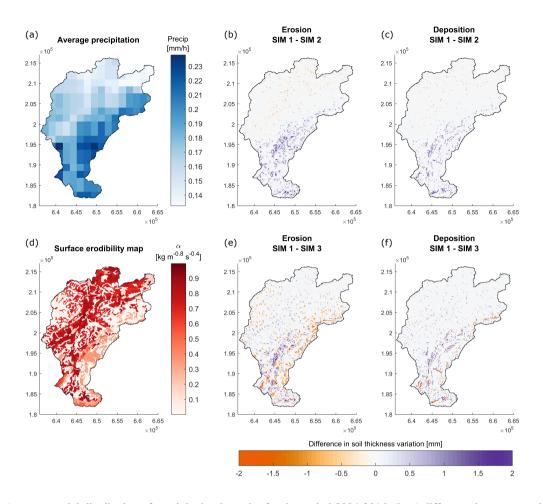
Figure 7. (a) Average spatial distribution of precipitation intensity for the period 2004-2016, (b, c) difference between erosion/deposition generated by distributed and uniform rainfall in 13 years, (d) spatial distribution of calibrated surface erodibility α, (e, f) difference between erosion/deposition generated by distributed and uniform surface erodibility in 13 years. A positive value indicates that uniform precipitation or surface erodibility determines less erosion/more deposition than variable precipitation or surface erodibility.

1. Figures 7b and 7c show the difference between the variable and uniform precipitation maps for erosion and deposition, respectively. Similarly, Figures 7e and 7f show the difference between the variable and uniform surface erodibility maps for erosion and deposition separately.

The results show that with uniform precipitation, erosion and deposition are reduced in the south-eastern part of the basin and increased in the north-western (Figure 7b and 7c). The overall patterns reflect the average spatial distribution of precipitation in the Kleine Emme catchment for the years 2003-2016, with the highest mean rain intensities associated with more erosion (Figure 7a). Uniform surface erodibility increases sediment erosion and deposition in the forested areas and reduces them in crop areas (Figure 7e and 7f). In both cases, the overall effect of removing the spatial variability in erosion drivers is a more uniform distribution of the sediment source areas across the basin.
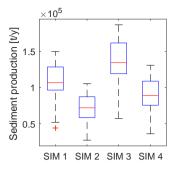
Figure 8. Sediment production in the basin as total sediment detached annually for the four simulations. Boxplots (median, interquartile range and outliers) show the internal variability in the period 2004-2016.

To quantify the erosional power of the four combinations of erosion drivers, we computed the total sediment mass detached yearly across the whole basin (referred to as sediment production) in the four simulations. The distribution of the yearly sediment production with interannual variability is reported in Figure 8. We observe that the removal of spatial variability generates two opposite effects for precipitation and surface erodibility. Sediment production increases when removing the spatial variability in surface erodibility and decreases when removing the spatial variability in precipitation, coherently with the reduced erosive power observed in Figure 6. In SIM 4 the balance between the two opposing effects determines a slight overall reduction in sediment production. The differences between the scenarios are within natural interannual variability in sediment production, but they are all statistically significant for change in median.

4.3 Connectivity of sediment transfer

The connectivity of sediment transfer, i.e sediment source areas linked to the river network, within the catchment for the different simulation configurations has been quantified by means of the sediment delivery ratio (SDR). The SDR is defined according to Walling (1983) as the ratio of the sediment delivered at the outlet of a selected area to the gross erosion in that area. The mean annual SDRs, which were computed at the outlet point of the main tributaries and at several cross-sections along the main channel, are reported in Figure 9 as a function of the drainage area.

Sediment connectivity along the main channel shows an increasing trend as a function of the upstream area for all simulations (Figure 9c). This trend is explained by the higher SDR of the tributaries compared to that of the main channel (Figure 9b) and by the absence of significant sediment sinks in the main channel. For the subbasins with outlets along the main channel, removing the spatial variability in surface erodibility (SIM 3) has the overall effect to increase sediment connectivity. In some tributaries, however, the opposite effect is observed (T5 and T6). Finally, Figure 9c shows that removing the spatial variability in precipitation (SIM 2 and 4) also increases the SDR, therefore sediment connectivity (compared to SIM 1 and 3, respectively).
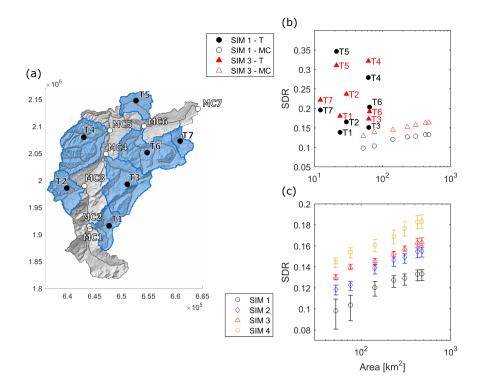
Figure 9. (a) Locations where the sediment delivery ratio has been computed: at the outlet of the main tributaries (T) and along the main channel (MC), (b) mean annual SDR vs drainage area for tributaries and points along the main channel for distributed rainfall simulations, (c) comparison of mean annual SDRs at the main channel points for the four simulations. The error bars show the interquartile range of the annual SDR variability.

4.4 Sediment loads and initial soil moisture

The distribution of annual sediment yields at the outlet generated by the four simulation experiments showed that distributed precipitation simulations (SIM 1 and 3) generated higher sediment loads than their uniform precipitation equivalents (SIM 2 and 4) (Figure 10a). Distributed erodibility (SIM 1 and 2) produced smaller sediment loads than uniform erodibility (SIM 3 and 4).

To further investigate the differences among the sediment yield distributions, in Figure 10b we show the influence of spatial variability in rainfall and surface erodibility on event-based sediment yields for high and low initial soil moisture (SM_0) conditions. After separating the outlet hydrograph into single events, we computed the total sediment yields for each event and compared the distributions of the events with high and low initial soil moisture. Low SM_0 events are defined as those with SM_0 smaller than the 20th percentile of the SM_0 distribution; high SM_0 events have a SM_0 greater than the 80th percentile. The hydrological model performance for these events is good and comparable to the entire simulation performance, however it indicates a tendency to overestimation especially for low SM_0 events (see Table S2 and Figure S3).
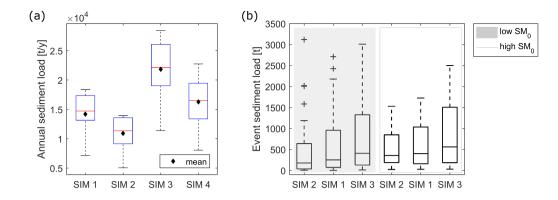
Figure 10. (a) Boxplots of annual sediment load and their mean values at the outlet of the catchment in the four simulation experiments, (b) boxplots of event sediment loads divided into low and high initial soil moisture conditions. The boxplots compare the effect of the spatial variability in precipitation and surface erodibility on events with different initial soil moisture.

The distributions of event sediment yields largely overlap, however it is possible to observe that it is more affected by the precipitation spatial variability when SM_0 is low. The differences between the median, 25th and 75th percentile of the SIM 1 and 2 are bigger for low SM_0 than for high SM_0. On the contrary, removing variability in surface erodibility seems to equally affect low and high initial SM_0 events (Figure 10b).

5   Discussion

5.1   Sources of concentration variability

The modelling approach presented here can reproduce part of the observed SSC-Q scatter, implying that it contains some of the relevant sources of sediment concentration variability in the hydrological and sediment production processes at the catchment scale (Figure 3b). However, it also highlights that to fully capture the scatter, other sources should be included.

The sources of variability accounted for by our deterministic modelling of the hydrology and sediment transfer are the time-varying meteorological inputs and the spatially distributed nature of the model. The precipitation input combines both temporal and spatial components of variability. The temporal component is visible in Figure 5a, showing that the same sediment concentration can correspond to a large range of discharge values, depending on the type of event and the initial soil wetness conditions that precede it. Spatial variability in precipitation contributes to the SSC-Q scatter, by increasing the flow variability itself (Figure 6c) and by allowing the same discharge at the outlet to be generated by many combinations of overland flow situations over the hillslopes. Each of these combinations activates different sediment sources that have a characteristic hydrological and sediment signal and connectivity to the river network. In particular, we identify localized high-intensity summer storms as a main source of scatter, while snowmelt and winter storms produce a more homogeneous response throughout

the basin. The spatially variable surface erodibility can additionally contribute to the uniqueness of the sediment signals of the activated source areas, when its spatial distribution is such to enhance the topographic heterogeneity within the basin.

Other sources of variability in sediment transport are implicit in the spatially distributed nature of the model, which allows to account for the heterogeneity of topography, soil depth and soil properties at very high resolution. These heterogeneities are responsible for the residual scatter of SIM 4, where the variability of both erosion drivers have been removed.

It is worth noting that, because the sediment storage on hillslope cells is not exhausted during our simulation experiments, sediment availability does not influence sediment production in our study. Therefore, sediment availability in the simulation experiments does not drive changes in the dominant sediment sources and does not add spatial variability to the sediment response.

The main limitation of our approach in reproducing SSC variability is, however, the lack of processes representing very localized sediment sources, which are usually characterized by a threshold behavior and therefore diversify the local sediment response. In this respect, Schwab et al. (2008) showed that in the Kleine Emme basin short time scale threshold processes are responsible for the export of regolith produced by soil creep in landslides. The absence of these processes in our model is likely the main reason for the smaller-than-observed modelled SSC-Q scatter, but also for the underestimation of the highest SSCs, the soil erosion rate and annual sediment load, presented in section 4.1. Finally, we acknowledge that also inherent stochasticity in the sediment mobilization and transfer are responsible for part of the observed SSC-Q rating curve scatter (e.g. Fuller et al., 2003; Malmon et al., 2003). This inherent stochasticity cannot be reproduced by our modelling approach with deterministic simulation, but it can be included with stochastic simulation experiments and a probabilistic framework (e.g. Bennett et al., 2014). We are working on overcoming these limitations in future research.

5.2   Spatial organization of suspended sediment transport

The explicit combination of hydrological processes and topographic and land use effects in the model can help to investigate the spatial organization of sediment transport, and in particular, how this is affected by the spatial variability in erosion drivers. Spatial variability enhances the heterogeneity of erosion and deposition across the catchment, thus favoring the clustering of sediment source areas (Figure 7). Sediment production is increased by the spatially variable precipitation (SIM 1 and SIM 3), due to increased erosive power (Figure 8). The effect of a spatially variabile surface erodibility depends on the distribution of overland flow relative to that of surface erodibility and, in this case, the lower sediment productions of SIM 1 and 2 (Figure 8) indicate that the two distributions combine more intense overland flow with lower erodibility areas, thus reducing the overall sediment production.

In Figure 9 we use the modelled SDR as a measure of sediment transfer connectivity, as it quantifies the proportion of mobilized sediment that is routed to the outlet of a selected subbasin by action of overland and channel flow. As such, the modelled SDR can be seen as a dynamic indicator of functional connectivity, where the discharge is represented explicitly in time and space as a function of the hydrological forcings and topographic characteristics, as opposed to the widely used approximation as a function of the upstream area. In this way, our approach integrates the variability of functional connectivity

385 both in time and space. A comparable approach to dynamically quantify the functional connectivity has been proposed by Mahoney et al. (2018), which is also based on hydrological modelling.

As shown by the sediment delivery ratio, the connectivity of sediment sources is reduced by the spatial variability of precipitation and this effect can be explained by the geomorphic connectivity of the catchment. The concentration of the distributed precipitation, the shallower soils and steeper slopes in the southeastern region of the basin, i.e. tributaries T1, T3, T6 and the

390 upper stretch of the main channel (see Figure 9a), favor overland flow generation, and thus hydrological connectivity. However, the lower topographic connectivity of these subbasins overall determines a reduction in the sediment transfer connectivity. Such lower connectivity is indicated by the low SDRs of these subbasins in SIM 3, which does not account for the land use effect, and suggests the presence of geomorphic sediment buffers (Fryirs, 2013). The different topographic connectivity of the southeastern and northwestern regions reflects the different geomorphology of these two parts of the basin. In fact, the southeastern

395 region of the basin is characterized by a predominantly Last Glacial Maximum landscape with wide valleys and major instabilities, which are in most cases not directly connected to the river network (Schwab et al., 2008; Van Den Berg et al., 2012; Clapuyt et al., 2019). On the other hand, the northwestern part of the basin, i.e. tributaries T4 and T5, shows a rejuvenating landscape where recent fluvial dissection created narrow and deeply incised valleys with a strong coupling between hillslopes and channels (Schlunegger and Schneider, 2005; Norton et al., 2008).

400 The reduction of sediment transfer connectivity by spatially distributed surface erodibility can be attributed to the assumption in the sediment module that sediment discharge is always in equilibrium with the overland flow transport capacity. Based on this assumption, a spatially variable α allows, on the one hand to modulate the sediment mobilization in space and, on the other hand, to define preferential areas of sediment deposition and therefore sediment connectivity. By associating a lower transport capacity to forests, their role as sediment buffers blocking sediments will emerge. Vice versa, high α values in crop areas will

405 mean the absence of obstacles to sediment flux. Therefore, the smaller sediment transfer connectivity of SIM 1 and 2 compared to SIM 3 and 4 reflects the location of sediment buffers (i.e. forests) with respect to the channel network. In fact, in most of the basin, forested areas surround channel headwaters, thus disconnecting the sediment sources on the hillslopes and mountain flanks from the river network (see e.g. Clinnick, 1985; Parkyn et al., 2005; Schoonover et al., 2006; Mekonnen et al., 2015).

5.3 Sediment load and connectivity

410 The analyses presented in the previous sections focus on the driving processes of sediment mobilization and transfer across the basin and the reasons for the reduction in SDR with variable erosion drivers. In this section we analyse how their balance determines the sediment load at the outlet.

In the distributed surface erodibility simulations (SIM 1 and 2) a reduced sediment yield (Y) is observed at the basin outlet and it is determined by a reduction in both sediment production (P) and sediment transfer connectivity (expressed by the SDR)

415 with respect to uniform erodibility simulations (SIM 3 and 4):

$$\downarrow Y = SDR \downarrow \cdot P \downarrow . \tag{6}$$

In the distributed precipitation simulations (SIM 1 and 3) instead, an increased sediment yield at the basin outlet is observed compared to uniform precipitation simulations, which results from a combination of a smaller SDR and a much greater sediment production across the basin. The increase in sediment yield indicates that the greater sediment production dominates over the decreased sediment connectivity:

$$\uparrow Y = SDR \downarrow \cdot P \Uparrow . \tag{7}$$

This result means that the localized sediment source areas are triggered by the very high erosive power of localised precipitation captured by distributed simulations. Their signal reaches the outlet despite the system is globally less efficient in evacuating the eroded sediments. These hotspots of erosion are generated where precipitation falls with a high intensity, soil saturation is reached soon during storms, eventually favoured by shallow soils, and therefore hydrological and sediment flux connectivity are locally high.

In a hydrological modeling experiment conducted with TOPKAPI-ETH on the same catchment, Paschalis et al. (2014) demonstrated the dependence of the discharge peak on the clustering of high soil moisture areas. Our results show that the high soil moisture areas may also define the sediment signal. This finding also suggests that a large proportion of the sediment yield can be supplied by just few localized sediment sources (e.g. Pelletier, 2012). The role of soil moisture in producing high sediment concentrations has also been highlighted by Dominic et al. (2015) and Brasington and Richards (2000), who attribute the peaks of SSCs to the connection of remote sediment sources during the wetting up of the catchment.

Given the relevance of soil moisture spatial distribution for runoff generation, we also expect event sediment yields to be more affected by the precipitation spatial variability, i.e. precipitation intensity, at low initial soil moisture than at high initial soil moisture, as it is suggested by Figure 10b. This is further supported by findings of Paschalis et al. (2014) and Shah et al. (1996) which indicate that higher initial basin saturation reduces the dependency of runoff on precipitation spatial distribution. However, we also highlight that in our study the relatively small difference between the sediment load distributions of low and high SM_0 events and the tendency to overestimate flow in low SM_0 events, do not allow for a clear conclusion.

6 Conclusions

We presented a new spatially distributed soil erosion and suspended sediment transport module integrated into the computationally efficient physically based hydrological model TOPKAPI-ETH. The model allows for continuous long-term, high temporal and spatial resolution simulations of erosion and sediment transport by overland flow on hillslope and in channels in medium to large basin. With the aim of exploring the impacts of two key spatially variable erosion drivers on suspended sediment dynamics, we conducted a series of numerical experiments on a mesoscale river basin. We compared the effects of spatially variable rainfall and surface erodibility with combinations of uniform and variable spatial distributions of these drivers.

Our results show that, first, the proposed model can reproduce part of the scatter of the observed SSC-Q relation, which is generated by spatially and temporally variable meteorological inputs and spatial heterogeneities of the physical properties

of the basin, leading to a multitude of possible flow and sediment pathways. At the same time, our results suggest that other
450 processes are also relevant to capture the scatter, such as localized sediment sources and the inherent randomness of sediment production and transfer, which are not included in our model.

Second, we found that spatial variability in both drivers favors the clustering of sediment source areas and reduces their overall connectivity to the river network, by capturing the buffering effect of forests and low slope areas. At the same time, spatially variable surface erodibility reduces sediment production, while a spatially variable precipitation increases sediment
455 production by high rates of erosion in areas of high rainfall and overland flow intensity.

Third, we found that the combination of the effects of spatial variability on sediment production and connectivity determines an overall lower sediment yield for surface erodibility, due to reduced sediment production and to buffering effects, and a greater sediment yield for precipitation, due to locally very high soil erosion. This last result is due to areas of high soil moisture in the catchment that are easy to saturate, which produce high local sediment inputs and catchment loads in spatially
460 variable simulations.

Although our findings were obtained with reference to the specific climatic and geomorphologic feature of the Kleine Emme catchment, we think they indicate the general importance of resolving the spatial variability in sediment mobilization and transfer processes when modelling sediment dynamics at the basin scale. The model we presented is particularly suitable for applications at medium and large scales, where gradients in climatic and physiographic characteristics represent a key
465 control of sediment mobilization and transfer. Moreover, this model offers a valuable tool for investigating future scenarios of precipitation and land cover, which are expected to take place due to climate change or human land use management.

Data availability. DEM, soil and land use maps, discharge and suspended sediment concentrations data and simulation results are available at https://doi.org/10.3929/ethz-b-000358874. Meteorological input data can be requested at https://gate.meteoswiss.ch/idaweb/login.do.

Author contributions. GB developed the model, carried out the simulations and the analyses of the results. PM and PB contributed to the
470 conceptualization of the model and to the discussion of the results. GB prepared the manuscript with contributions and edits from all co-authors.

Competing interests. The authors declare that they have no conflict of interest.

Acknowledgements. We thank Fritz Schlunegger for sharing his knowledge of the study basin. The study was funded by the DAFNE project, an Horizon 2020 programme WATER 2015 of the European Union, GA no. 690268.

References

Asselman, N. E.: Suspended sediment dynamics in a large drainage basin: The River Rhine, Hydrological Processes, 13, 1437–1450, https://doi.org/10.1002/(SICI)1099-1085(199907)13:10<1437::AID-HYP821>3.0.CO;2-J, 1999.

Asselman, N. E.: Fitting and interpretation of sediment rating curves, Journal of Hydrology, 234, 228–248, https://doi.org/10.1016/S0022-1694(00)00253-5, 2000.

Beasley, D. B., Huggins, L. F., and Monke, E. J.: ANSWERS: A Model for Watershed Planning, Transactions of the ASAE, 23, 0938–0944, https://doi.org/10.13031/2013.34692, http://elibrary.asabe.org/abstract.asp??JID=3&AID=34692&CID=t1980&v=23&i=4&T=1, 1980.

Bennett, G. L., Molnar, P., McArdell, B. W., and Burlando, P.: A probabilistic sediment cascade model of sediment transfer in the Illgraben, Water Resources Research, 50, 1225–1244, https://doi.org/10.1002/2013WR013806, http://doi.wiley.com/10.1002/2013WR013806, 2014.

Bilotta, G. S. and Brazier, R. E.: Understanding the influence of suspended solids on water quality and aquatic biota, Water Research, 42, 2849–2861, https://doi.org/10.1016/j.watres.2008.03.018, 2008.

Bodeneignungskarte: 77.2 Digitale Bodeneignungskarte der Schweiz, https://www.blw.admin.ch/blw/de/home/politik/datenmanagement/geografisches-informationssystem-gis/download-geodaten.html, 2012.

Borrelli, P., Robinson, D. A., Fleischer, L. R., Lugato, E., Ballabio, C., Alewell, C., Meusburger, K., Modugno, S., Schütt, B., Ferro, V., Bagarello, V., Oost, K. V., Montanarella, L., and Panagos, P.: An assessment of the global impact of 21st century land use change on soil erosion, Nature Communications, 8, https://doi.org/10.1038/s41467-017-02142-7, http://dx.doi.org/10.1038/s41467-017-02142-7, 2017.

Bracken, L. J., Turnbull, L., Wainwright, J., and Bogaart, P.: Sediment connectivity: A framework for understanding sediment transfer at multiple scales, Earth Surface Processes and Landforms, 40, 177–188, https://doi.org/10.1002/esp.3635, 2015.

Brasington, J. and Richards, K.: Turbidity and suspended sediment dynamics in small catchments in the Nepal Middle Hills, Hydrological Processes, 14, 2559–2574, https://doi.org/10.1002/1099-1085(20001015)14:14<2559::AID-HYP114>3.0.CO;2-E, 2000.

Chen, X. and Zong, Y.: Coastal Erosion Along the Changjiang Deltaic Shoreline, China: History and Prospective, Estuarine, Coastal and Shelf Science, 46, 733–742, https://doi.org/10.1006/ecss.1997.0327, https://linkinghub.elsevier.com/retrieve/pii/S0272771497903279, 1998.

Clapuyt, F., Vanacker, V., Schlunegger, F., Christl, M., and Van Oost, K.: Spatio-temporal dynamics of sediment transfer systems in landslide-prone alpine catchments, Solid Earth Discussions, pp. 1–22, https://doi.org/10.5194/se-2018-139, 2019.

CLC: Corine Land Cover (CLC) map 2012, https://land.copernicus.eu/pan-european/corine-land-cover/clc-2012, 2014.

Clinnick, P. F.: Buffer strip management in forest operations: A review, Australian Forestry, 48, 34–45, https://doi.org/10.1080/00049158.1985.10674421, 1985.

Cohen, S., Kettner, A. J., Syvitski, J. P., and Fekete, B. M.: WBMsed, a distributed global-scale riverine sediment flux model: Model description and validation, Computers and Geosciences, 53, 80–93, https://doi.org/10.1016/j.cageo.2011.08.011, 2013.

Collins, A. L. and Walling, D. E.: Progress in Physical Geography Documenting catchment suspended sediment sources : problems , approaches and prospects, Progress in Physical Geography, 2, 159–196, https://doi.org/10.1191/0309133304pp409ra, 2004.

Costa, A., Anghileri, D., and Molnar, P.: Hydroclimatic control on suspended sediment dynamics of a regulated Alpine catchment: A conceptual approach, Hydrology and Earth System Sciences, 22, 3421–3434, https://doi.org/10.5194/hess-22-3421-2018, 2018.

Coulthard, T. J., Neal, J. C., Bates, P. D., Ramirez, J., de Almeida, G. A., and Hancock, G. R.: Integrating the LISFLOOD-FP 2D hydrodynamic model with the CAESAR model: Implications for modelling landscape evolution, Earth Surface Processes and Landforms, 38, 1897–1906, https://doi.org/10.1002/esp.3478, 2013.

Davies-Colley, R. J. and Smith, D. G.: Turbidity, suspended sediment, and water clarity: A review, Journal of the American Water Resources Association, 37, 1085–1101, https://doi.org/10.1111/j.1752-1688.2001.tb03624.x, 2001.

Dominic, J. A., Aris, A. Z., and Sulaiman, W. N. A.: Factors Controlling the Suspended Sediment Yield During Rainfall Events of Dry and Wet Weather Conditions in A Tropical Urban Catchment, Water Resources Management, 29, 4519–4538, https://doi.org/10.1007/s11269-015-1073-0, 2015.

Doten, C. O., Bowling, L. C., Lanini, J. S., Maurer, E. P., and Lettenmaier, D. P.: A spatially distributed model for the dynamic prediction of sediment erosion and transport in mountainous forested watersheds, Water Resources Research, 42, 1–15, https://doi.org/10.1029/2004WR003829, 2006.

Dürst Stucki, M., Schlunegger, F., Christener, F., Otto, J. C., and Götz, J.: Deepening of inner gorges through subglacial meltwater - An example from the UNESCO Entlebuch area, Switzerland, Geomorphology, 139-140, 506–517, https://doi.org/10.1016/j.geomorph.2011.11.016, http://dx.doi.org/10.1016/j.geomorph.2011.11.016, 2012.

Duvert, C., Gratiot, N., Evrard, O., Navratil, O., Némery, J., Prat, C., and Esteves, M.: Drivers of erosion and suspended sediment transport in three headwater catchments of the Mexican Central Highlands, Geomorphology, 123, 243–256, https://doi.org/10.1016/j.geomorph.2010.07.016, http://dx.doi.org/10.1016/j.geomorph.2010.07.016, 2010.

Fatichi, S., Rimkus, S., Burlando, P., Bordoy, R., and Molnar, P.: High-resolution distributed analysis of climate and anthropogenic changes on the hydrology of an Alpine catchment, Journal of Hydrology, 525, 362–382, https://doi.org/10.1016/j.jhydrol.2015.03.036, http://dx.doi.org/10.1016/j.jhydrol.2015.03.036, 2015.

Ferguson, R. I.: River Loads Underestimated by Rating Curves, Water Resources Research, 22, 74–76, https://doi.org/10.1029/WR022i001p00074, 1986.

Francipane, A., Ivanov, V. Y., Noto, L. V., Istanbulluoglu, E., Arnone, E., and Bras, R. L.: TRIBS-Erosion: A parsimonious physically-based model for studying catchment hydro-geomorphic response, Catena, 92, 216–231, https://doi.org/10.1016/j.catena.2011.10.005, http://dx.doi.org/10.1016/j.catena.2011.10.005, 2012.

Frei, C. and Schär, C.: A precipitation climatology of the Alps from high-resolution rain-gauge observations, International Journal of Climatology, 18, 873–900, https://doi.org/10.1002/(SICI)1097-0088(19980630)18:8<873::AID-JOC255>3.0.CO;2-9, http://doi.wiley.com/10.1002/%28SICI%291097-0088%2819980630%2918%3A8%3C873%3A%3AAID-JOC255%3E3.0.CO%3B2-9, 1998.

Fryirs, K.: (Dis)Connectivity in catchment sediment cascades: A fresh look at the sediment delivery problem, Earth Surface Processes and Landforms, 38, 30–46, https://doi.org/10.1002/esp.3242, 2013.

Fryirs, K. and Brierley, G. J.: Slope – channel decoupling in Wolumla catchment , New South Wales, Australia : the changing nature of sediment sources following European settlement, Catena, 35, 41–63, https://doi.org/https://doi.org/10.1016/S0341-8162(98)00119-2, https://www.sciencedirect.com/science/article/pii/S0341816298001192, 1999.

Fryirs, K., Brierley, G. J., Preston, N. J., and Spencer, J.: Catchment-scale (dis)connectivity in sediment flux in the upper Hunter catchment, New South Wales, Australia, Geomorphology, 84, 297–316, https://doi.org/10.1016/j.geomorph.2006.01.044, 2007.

Fuller, C. W., Willett, S. D., Hovius, N., and Slingerland, R.: Erosion Rates for Taiwan Mountain Basins: New Determinations from Suspended Sediment Records and a Stochastic Model of Their Temporal Variation, The Journal of Geology, 111, 71–87, https://doi.org/10.1086/344665, 2003.

Gao, P.: Understanding watershed suspended sediment transport, Progress in Physical Geography, 32, 243–263, https://doi.org/10.1177/0309133308094849, 2008.

Hancock, G., Evans, K., Willgoose, G., Moliere, D., Saynor, M., and Loch, R.: Medium-term erosion simulation of an abandoned mine site using the SIBERIA landscape evolution model, Australian Journal of Soil Research, 38, 249–263, 2000.

Hancock, G. R., Webb, A. A., and Turner, L.: Sediment transport in forested head water catchments – Calibration and validation of a soil erosion and landscape evolution model, Journal of Hydrology, 554, 12–23, https://doi.org/10.1016/j.jhydrol.2017.08.049, http://dx.doi.org/10.1016/j.jhydrol.2017.08.049, 2017.

Heckmann, T., Cavalli, M., Cerdan, O., Foerster, S., Javaux, M., Lode, E., Smetanová, A., Vericat, D., and Brardinoni, F.: Indices of sediment connectivity: opportunities, challenges and limitations, Earth-Science Reviews, pp. 1–32, https://doi.org/10.1016/j.earscirev.2018.08.004, https://doi.org/10.1016/j.earscirev.2018.08.004, 2018.

Hinderer, M., Kastowski, M., Kamelger, A., Bartolini, C., and Schlunegger, F.: River loads and modern denudation of the Alps - A review, Earth-Science Reviews, 118, 11–44, https://doi.org/10.1016/j.earscirev.2013.01.001, http://dx.doi.org/10.1016/j.earscirev.2013.01.001, 2013.

Horowitz, A. J.: An evaluation of sediment rating curves for estimating suspended sediment concentrations for subsequent flux calculations, Hydrological Processes, 17, 3387–3409, https://doi.org/10.1002/hyp.1299, 2003.

Kasten, F. and Czeplak, G.: Solar and terrestrial radiation dependent on the amount and type of cloud, Solar Energy, 24, 177–189, https://doi.org/10.1016/0038-092X(80)90391-6, 1980.

Kondolf, G. M.: Hungry water: Effects of dams and gravel mining on river channels, Environmental Management, 21, 533–551, https://doi.org/10.1007/s002679900048, 1997.

Lang, A., Bork, H.-R., and Preston, N.: Changes in sediment flux and storage within a fluvial system : some examples from the Rhine catchment, Hydrological Processes, 3334, 3321–3334, https://doi.org/10.1002/hyp.1389, 2003.

Liu, Z. and Todini, E.: Towards a comprehensive physically-based rainfall-runoff model, Hydrology and Earth System Sciences, 6, 859–881, https://doi.org/10.5194/hess-6-859-2002, http://www.hydrol-earth-syst-sci.net/6/859/2002/, 2002.

Mahoney, D. T., Fox, J. F., and Al Aamery, N.: Watershed erosion modeling using the probability of sediment connectivity in a gently rolling system, Journal of Hydrology, 561, 862–883, https://doi.org/10.1016/j.jhydrol.2018.04.034, https://doi.org/10.1016/j.jhydrol.2018.04.034, 2018.

Malmon, D. V., Dunne, T., and Reneau, S. L.: Stochastic Theory of Particle Trajectories through Alluvial Valley Floors, The Journal of Geology, 111, 525–542, https://doi.org/10.1086/376764, 2003.

Mekonnen, M., Keesstra, S. D., Stroosnijder, L., Baartman, J. E., and Maroulis, J.: Soil Conservation Through Sediment Trapping: A Review, Land Degradation and Development, 26, 544–556, https://doi.org/10.1002/ldr.2308, 2015.

Misset, C., Recking, A., Legout, C., Poirel, A., Cazilhac, M., Esteves, M., and Bertrand, M.: An attempt to link suspended load hysteresis patterns and sediment sources configuration in alpine catchments, Journal of Hydrology, 576, 72–84, https://doi.org/10.1016/j.jhydrol.2019.06.039, https://doi.org/10.1016/j.jhydrol.2019.06.039, 2019.

Montgomery, D. R.: Soil erosion and agricultural sustainability, Proceedings of the National Academy of Sciences, 104, 13 268–13 272, https://doi.org/10.1073/pnas.0611508104, 2007.

Nearing, M. A., Foster, G. R., Lane, L. J., and Finkner, S. C.: A Process-Based Soil Erosion Model for USDA-Water Erosion Prediction Project Technology, Transactions of the ASAE, 32, 1587–1593, 1989.

Nearing, M. A., Pruski, F. F., and O'Neal, M. R.: Expected climate change impacts on soil erosion rates: A review, Journal of Soil and Water Conservation, 59, 43–50, 2004.

Norton, K. P., von Blanckenburg, F., Schlunegger, F., Schwab, M., and Kubik, P. W.: Cosmogenic nuclide-based investigation of spatial erosion and hillslope channel coupling in the transient foreland of the Swiss Alps, Geomorphology, 95, 474–486, https://doi.org/10.1016/j.geomorph.2007.07.013, 2008.

590   Olarieta, J. R., Besga, G., Rodríguez, R., Usón, A., Pinto, M., and Virgel, S.: Sediment enrichment ratios after mechanical site preparation for Pinus radiata plantation in the Basque Country, Geoderma, 93, 255–267, 1999.

Pappas, C., Fatichi, S., Rimkus, S., Burlando, P., and Huber, M. O.: The role of local-scale heterogeneities in terrestrial ecosystem modeling, Journal of Geophysical Research: Biogeosciences, 120, 341–360, https://doi.org/10.1002/2014JG002735, 2015.

Parkyn, S. M., Davies-Colley, R. J., Cooper, A. B., and Stroud, M. J.: Predictions of stream nutrient and sediment yield changes following restoration of forested riparian buffers, Ecological Engineering, 24, 551–558, https://doi.org/10.1016/j.ecoleng.2005.01.004, 2005.

595   Paschalis, A., Fatichi, S., Molnar, P., Rimkus, S., and Burlando, P.: On the effects of small scale space-time variability of rainfall on basin flood response, Journal of Hydrology, 514, 313–327, https://doi.org/10.1016/j.jhydrol.2014.04.014, http://dx.doi.org/10.1016/j.jhydrol.2014.04.014, 2014.

Peleg, N., Skinner, C., Fatichi, S., and Molnar, P.: Temperature effects on heavy rainfall modify catchment hydro-morphological response, Earth Surface Dynamics, In Review, 1–34, 2019.

600   Pelletier, J. D.: A spatially distributed model for the long-term suspended sediment discharge and delivery ratio of drainage basins, Journal of Geophysical Research: Earth Surface, 117, 1–15, https://doi.org/10.1029/2011JF002129, 2012.

Peucker-Ehrenbrink, B.: Land2Sea database of river drainage basin sizes, annual water discharges, and suspended sediment fluxes, Geochemistry, Geophysics, Geosystems, 10, 1–10, https://doi.org/10.1029/2008GC002356, 2009.

Pimentel, D., Allen, J., Beers, A., Guinand, L., Linder, R., McLaughlin, P., Meer, B., Musonda, D., Perdue, D., Poisson, S., Siebert, S.,

605   Stoner, K., Salazar, R., and Hawkins, A.: World Agriculture and Soil Erosion, BioScience, 37, 277–283, https://doi.org/10.2307/1310591, 1987.

Prosser, I. P. and Rustomji, P.: Sediment transport capacity relations for overland flow, Progress in Physical Geography, 24, 179–193, https://doi.org/10.1177/030913330002400202, http://journals.sagepub.com/doi/10.1177/030913330002400202, 2000.

Rickenmann, D., Badoux, A., and Hunzinger, L.: Significance of sediment transport processes during piedmont floods: The 2005 flood events

610   in Switzerland, Earth Surface Processes and Landforms, 41, 224–230, https://doi.org/10.1002/esp.3835, 2016.

Schlunegger, F. and Schneider, H.: Relief-rejuvenation and topographic length scales in a fluvial drainage basin, Napf area, Central Switzerland, Geomorphology, 69, 102–117, https://doi.org/10.1016/j.geomorph.2004.12.008, 2005.

Schmidt, J. C. and Wilcock, P. R.: Metrics for assessing the downstream effects of dams, Water Resources Research, 44, https://doi.org/10.1029/2006WR005092, 2008.

615   Schmidt, S., Ballabio, C., Alewell, C., Panagos, P., and Meusburger, K.: Filling the European blank spot—Swiss soil erodibility assessment with topsoil samples, Journal of Plant Nutrition and Soil Science, 181, 737–748, https://doi.org/10.1002/jpln.201800128, 2018.

Schoonover, J. E., Williard, K. W. J., Zaczek, J. J., Mangun, J. C., and Carver, A. D.: Agricultural sediment reduction by giant cane and forest riparian buffers, Water, Air, and Soil Pollution, 169, 303–315, https://doi.org/10.1007/s11270-006-3111-2, 2006.

Schwab, M., Rieke-Zapp, D., Schneider, H., Liniger, M., and Schlunegger, F.: Landsliding and sediment flux in the

620   Central Swiss Alps: A photogrammetric study of the Schimbrig landslide, Entlebuch, Geomorphology, 97, 392–406, https://doi.org/10.1016/j.geomorph.2007.08.019, 2008.

Schwarb, M.: The alpine precipitation climate evaluation of a high-resolution analysis scheme using comprehensive rain-gauge data, ETH Zurich Research Collection, https://doi.org/10.3929/ethz-a-010782581, 2000.

Seeger, M., Errea, M. P., Beguería, S., Arnáez, J., Martí, C., and García-Ruiz, J. M.: Catchment soil moisture and rainfall characteristics as determinant factors for discharge/suspended sediment hysteretic loops in a small headwater catchment in the Spanish pyrenees, Journal of Hydrology, 288, 299–311, https://doi.org/10.1016/j.jhydrol.2003.10.012, 2004.

Shah, S. M., O'Connell, P. E., and Hosking, J. R.: Modelling the effects of spatial variability in rainfall on catchment response. 2. Experiments with distributed and lumped models, Journal of Hydrology, 175, 89–111, https://doi.org/10.1016/S0022-1694(96)80007-2, 1996.

Siakeu, J., Oguchi, T., Aoki, T., Esaki, Y., and Jarvie, H. P.: Change in riverine suspended sediment concentration in central Japan in response to late 20th century human activities, Catena, 55, 231–254, https://doi.org/10.1016/S0341-8162(03)00120-6, 2004.

Smith, B. P., Naden, P. S., Leeks, G. J., and Wass, P. D.: The influence of storm events on fine sediment transport, erosion and deposition within a reach of the River Swale, Yorkshire, UK, Science of the Total Environment, 314-316, 451–474, https://doi.org/10.1016/S0048-9697(03)00068-8, 2003.

SwissAlti3D: SwissAlti3D - The high precision digital elevation model of Switzerland, https://shop.swisstopo.admin.ch/en/products/height_models/alti3D, 2017.

Syvitski, J. and Kettner, A.: Sediment flux and the anthropocene, Philosophical Transactions of the Royal Society A: Mathematical, Physical and Engineering Sciences, 369, 957–975, https://doi.org/10.1098/rsta.2010.0329, 2011.

Syvitski, J., Vörösmarty, C. J., Kettner, A. J., and Green, P.: Impact of Humans on the Flux of Terrestrial Sediment to the Global Coastal Ocean, Science, 308, 376–380, https://doi.org/10.1126/science.1109454, http://www.sciencemag.org/cgi/doi/10.1126/science.1109454, 2005.

Tsuruta, K., Hassan, M. A., Donner, S. D., and Alila, Y.: Development and Application of a Large-Scale, Physically Based, Distributed Suspended Sediment Transport Model on the Fraser River Basin, British Columbia, Canada, Journal of Geophysical Research: Earth Surface, 123, 2481–2508, https://doi.org/10.1029/2017JF004578, 2018.

Van Den Berg, F., Schlunegger, F., Akçar, N., and Kubik, P.: 10Be-derived assessment of accelerated erosion in a glacially conditioned inner gorge, Entlebuch, Central Alps of Switzerland, Earth Surface Processes and Landforms, 37, 1176–1188, https://doi.org/10.1002/esp.3237, 2012.

Van Rompaey, A. J., Verstraeten, G., Van Oost, K., Govers, G., and Poesen, J.: Modelling mean annual sediment yield using a distributed approach, Earth Surface Processes and Landforms, 26, 1221–1236, https://doi.org/10.1002/esp.275, 2001.

Vercruysse, K., Grabowski, R. C., and Rickson, R. J.: Suspended sediment transport dynamics in rivers: Multi-scale drivers of temporal variation, Earth-Science Reviews, 166, 38–52, https://doi.org/10.1016/j.earscirev.2016.12.016, http://dx.doi.org/10.1016/j.earscirev.2016.12.016, 2017.

Wainwright, J., Turnbull, L., Ibrahim, T. G., Lexartza-Artza, I., Thornton, S. F., and Brazier, R. E.: Linking environmental régimes, space and time: Interpretations of structural and functional connectivity, Geomorphology, 126, 387–404, https://doi.org/10.1016/j.geomorph.2010.07.027, http://dx.doi.org/10.1016/j.geomorph.2010.07.027, 2011.

Walling, D. E.: Assessing the accuracy of suspended sediment rating curves for a small basin, Water Resources Research, 13, 531–538, https://doi.org/10.1029/WR013i003p00531, 1977.

Walling, D. E.: The sediment delivery problem, Journal of Hydrology, 65, 209–237, https://doi.org/10.1016/0022-1694(83)90217-2, 1983.

Walling, D. E.: Human impact on land-ocean sediment transfer by the world's rivers, Geomorphology, 79, 192–216, https://doi.org/10.1016/j.geomorph.2006.06.019, 2006.

Walling, D. E. and Webb, B. W.: The reliability of suspended sediment load data, Journal of the American Medical Association, 248, 2180, https://doi.org/10.1001/jama.248.17.2180, 1982.

Wass, P. D. and Leeks, G. J. L.: Suspended sediment Fluxes in the Humber catchment , UK, Hydrological Processes, 953, 1999.

Wittmann, H., von Blanckenburg, F., Kruesmann, T., Norton, K. P., and Kubik, P. W.: Relation between rock uplift and denudation from cosmogenic nuclides in river sediment in the Central Alps of Switzerland, Journal of Geophysical Research: Earth Surface, 112, 1–20, https://doi.org/10.1029/2006JF000729, 2007.

Woolhiser, D., Smith, R. E., and Goodrich, D.: A Kinematic Runoff and Erosion Model, 1990.

Yang, D., Kanae, S., Oki, T., Koike, T., and Musiake, K.: Global potential soil erosion with reference to land use and climate changes, Hydrological Processes, 17, 2913–2928, https://doi.org/10.1002/hyp.1441, 2003.

Yu, L.: The Huanghe (Yellow) River: A review of its development, characteristics, and future management issues, Continental Shelf Research, 22, 389–403, https://doi.org/10.1016/S0278-4343(01)00088-7, 2002.

Zabaleta, A., Martínez, M., Uriarte, J. A., and Antigüedad, I.: Factors controlling suspended sediment yield during runoff events in small headwater catchments of the Basque Country, Catena, 71, 179–190, https://doi.org/10.1016/j.catena.2006.06.007, 2007.